Development 135, 3053-3062 (2008) doi:10.1242/dev.022897

# Chato, a KRAB zinc-finger protein, regulates convergent extension in the mouse embryo

**María J. García-García[1,2,*], Maho Shibata[1] and Kathryn V. Anderson[2]**

In *Xenopus* and zebrafish embryos, elongation of the anterior-posterior body axis depends on convergent extension, a process that involves polarized cell movements and is regulated by non-canonical Wnt signaling. The mechanisms that control axis elongation of the mouse embryo are much less well understood. Here, we characterize the ENU-induced mouse mutation *chato*, which causes arrest at midgestation and defects characteristic of convergent extension mutants, including a shortened body axis, mediolaterally extended somites and an open neural tube. The *chato* mutation disrupts Zfp568, a Krüppel-associated box (KRAB) domain zinc-finger protein. Morphometric analysis revealed that the definitive endoderm of mouse wild-type embryos undergoes cell rearrangements that lead to convergent extension during early somite stages, and that these cell rearrangements fail in *chato* embryos. Although non-canonical Wnt signaling is important for convergent extension in the mouse notochord and neural plate, the results indicate that *chato* regulates body axis elongation in all embryonic tissues through a process independent of non-canonical Wnt signaling.

**KEY WORDS: Axis elongation, Convergent extension, Definitive endoderm, Morphogenesis, Mouse development**

## INTRODUCTION

In *Xenopus* and zebrafish, elongation of the anterior-posterior axis from a spherical early embryo depends on the movement and intercalation of lateral cells towards the midline, a process called convergent extension (reviewed by Wallingford et al., 2002). Extensive studies on intact embryos and tissue explants using time-lapse imaging have confirmed that coordinated cell rearrangements mediate convergent extension in fish and frog embryos (Concha and Adams, 1998; Davidson and Keller, 1999; Elul and Keller, 2000; Jessen et al., 2002; Keller and Tibbetts, 1989; Tahinci and Symes, 2003; Wallingford et al., 2000; Wilson and Keller, 1991).

Non-canonical Wnt signaling is required for convergent extension in *Xenopus* and zebrafish (reviewed by Tada et al., 2002). Genetic and experimental disruptions of this signaling pathway, such as loss of function mutations in zebrafish *van gogh-like 2* (*vangl2*; also known as *trilobite*) (Hammerschmidt et al., 1996; Jessen et al., 2002), or overexpression of mutated forms of *Dishevelled* in *Xenopus* (Goto and Keller, 2002; Moon et al., 1993; Tada and Smith, 2000; Wallingford et al., 2000), cause characteristic convergent extension defects, such as a short anterior-posterior axis, a wide notochord and a broad, open neural tube. Other genetic pathways are also important for convergent extension in zebrafish, including BMP gradients (von der Hardt et al., 2007), the zinc-finger protein Bloody fingers (Sumanas et al., 2005) and the ERRα orphan nuclear receptor (Bardet et al., 2005).

In the mouse, the morphogenetic events that create the elongated anterior-posterior body axis are not well understood. Elongation of the mouse embryo takes place during late gastrulation [embryonic day (E) 7.5-9.0], when extensive cell rearrangements/movements generate the germ layers and organ primordia (Kinder et al., 1999). As these cells reorganize and migrate, the embryo grows dramatically, from ~600 cells at pregastrula stages (E6.0) to nearly 14,000 at neurulation (E8.5) (Lawson, 1999). Recent time-lapse imaging studies showed that cell intercalation takes place in the axial midline of mouse embryos during the lengthening of the node along the anterior-posterior axis (Yamanaka et al., 2007). However, the importance of convergent extension movements to elongation of other embryonic tissues is not clear, in part owing to a lack of analysis of cell behavior during these stages.

Mouse mutants that lack components of the non-canonical Wnt signaling pathway show some of the features characteristic of *Xenopus* and zebrafish embryos with disrupted convergent extension, including a wide notochord and open neural tube (Greene et al., 1998; Kibar et al., 2001; Murdoch et al., 2001a). It has been proposed that defects in axial mesendoderm extension in mouse *Vangl2* [also known as loop-tail (*Lp*)] mutant embryos are caused by defective midline cell intercalation in the node area (Ybot-Gonzalez et al., 2007). Although it is clear that non-canonical Wnt signaling contributes to the elongation of the mammalian embryo (Wallingford et al., 2002; Wang, J. et al., 2006), the phenotypes of mouse mutants that lack non-canonical Wnt signaling are not as severe as those of their zebrafish mutant counterparts. For example, elongation and convergence of non-axial mesoderm is not as severely affected in mouse *Vangl2* embryos (Greene et al., 1998; Kibar et al., 2001; Murdoch et al., 2001a) as in zebrafish *vangl2* mutants (Hammerschmidt et al., 1996; Jessen et al., 2002), even though the mutations disrupt orthologous genes. Mouse mutants that lack non-canonical Wnt signaling die at birth with severe neurulation defects and disruption of planar cell polarity (PCP) in inner ear hair cells (Curtin et al., 2003; Montcouquiol et al., 2003; Wang, Y. et al., 2006), but their trunk length is similar to that of wild-type littermates and the contribution of PCP defects to mouse axis elongation is not clear. To date, the results suggest that convergent extension mechanisms controlled by non-canonical Wnt signaling are important for elongation of some embryonic tissues such as the notochord (Ybot-Gonzalez et al., 2007), but the differences between mouse and zebrafish *Vangl2* mutant phenotypes argue that other pathways and/or mechanisms contribute to the elongation of non-axial tissues in the mouse embryo.

[1]Molecular Biology and Genetics Department, Cornell University, Ithaca, NY 14853, USA. [2]Sloan Kettering Institute, New York, NY 10021, USA.

*Author for correspondence (e-mail: garciamj@cornell.edu)

**Accepted 10 July 2008**

Here we report the identification and characterization of Chato, a novel KRAB zinc-finger protein required for mammalian convergent extension. Two independent recessive mutant alleles of *chato* cause morphogenetic defects similar to those of fish and frog embryos with defective convergent extension, including a shorter and wider body axis, open neural tube and mediolaterally expanded somites. To evaluate whether *chato* regulates convergent extension mechanisms similar to those seen in fish and frogs, we measured changes in the length and width of wild-type and mutant embryonic tissues during early development. Because of the relative simplicity of its morphogenetic movements, we focused our analysis on the definitive endoderm layer, the precursor of the gut. Morphometric analysis of wild-type embryos shows that the definitive endoderm narrows and elongates during embryogenesis and that convergent extension of this tissue is mediated by cell rearrangements. In *chato* mutants, the definitive endoderm is wider and cell rearrangements do not take place. Genetic experiments indicate that Chato regulates convergent extension events through a novel pathway independent of non-canonical Wnt signaling.

## MATERIALS AND METHODS

### Mouse (*Mus musculus*) strains

The *chato* mutation was generated by ENU-mutagenesis as described previously (Garcia-Garcia et al., 2005; Kasarskis et al., 1998). *chato* was analyzed in C3H/FeJ, CAST/Ei and 129Sv/ImJ genetic backgrounds. *Nodal-lacZ* and *Lp* mice were obtained from Dr Elizabeth J. Robertson (Collignon et al., 1996b) and from Jackson Labs (LPT/LeJ strain) respectively. *Lp* mice were outcrossed to C3H/FeJ and genotyped with D1Mit36 and D1Mit149 SSLP markers.

### Physical mapping and sequencing of candidate genes

Genetic mapping of $Zfp568^{chato}$ was performed by linkage analysis of 981 opportunities for recombination with SSLP markers (www.informatics.jax.org and http://mouse.ski.mskcc.org). Physical map information was obtained from Ensembl (http://www.ensembl.org/Mus_musculus/index.html).

cDNAs of all candidate genes in the *chato* interval (*Zfp27*, *Zfp74*, *Zfp568*, *Zfp14*, *Zfp82* and *Zfp260*) were amplified by RT-PCR (Superscript One-Step RT-PCR, Invitrogen) using RNA from E8.5 *chato* and C57BL/6J (control) embryos. Amplification products were sequenced. A mutation, T to C, was identified at codon 64 of the *Zfp568* ORF. This point mutation generated an *Msp*I restriction fragment length polymorphism that was used to confirm linkage with *chato* embryos and carrier animals. No mutations were found in any of the other genes in the interval.

### Characterization of the $Zfp568^{RRU161}$ allele

BayGenomics RRU161 gene trap creates an abnormal splicing between the first coding exon of *Zfp568* and a splicing acceptor site present in the gene-trap vector (http://www.genetrap.org). *RRU161* completely disrupts the normal splicing of *Zfp568*, as tested by RT-PCR of homozygote RRU161 embryos using primers located in the first and second coding exons of *Zfp568*. The RRU161 gene-trap fusion protein contains 11 amino acids from Zfp568 followed by 19 amino acids that do not contain any recognizable functional domains (β-galactosidase coding sequence was out of frame).

### Analysis of mutant embryos

Embryos were dissected in PBS containing 0.4% BSA at different stages as assessed by presence of vaginal plugs in mothers. Whole-mount RNA in situ hybridization and staining for β-galactosidase activity were performed as described (Belo et al., 1997; Nagy, 2003).

Embryos used for length and width measurements were fixed in 4% paraformaldehyde at 4°C for 8-10 hours, then washed and photographed in PBS (dehydration was avoided to prevent shrinkage of embryos). Measurements were taken with Axiovision AC Zeiss software on pictures of the same magnification.

For immunohistochemistry and TUNEL, embryos were cryosectioned (8-10 μm) as previously described (Garcia-Garcia and Anderson, 2003). Antibodies used were anti-E-cadherin (cadherin 1) (Sigma) at 1/250 and anti-phospho-histone H3 (Ser10) (Upstate) at 1/250. TUNEL was performed using the ApopTag Detection Kit (Chemicon). As positive controls for TUNEL, we used sections treated with DNase I.

Cell counts were collected from embryos processed through *Ttr* in situ hybridization, embedding, cryosectioning (8 μm) and counterstaining with Fast Red. Data plots and statistical analysis of measurements were performed using Excel software (Microsoft). Statistical significance was calculated using two-tailed *t*-tests with Prism software (GraphPad).

Scanning electron microscopy was performed at Sloan-Kettering and Cornell Imaging Facilities using Jeoul and Hitachi 4500 microscopes. Samples were fixed overnight in PBS containing 2.5% glutaraldehyde, washed in PBS, dehydrated in ethanol and processed for critical-point drying and gold-palladium coating.

## RESULTS

### *chato* mutants fail to elongate the anterior-posterior axis

The *chato* mutation was isolated in a mutagenesis screen designed to identify recessive mutations that alter embryonic morphology at midgestation (Garcia-Garcia et al., 2005; see Materials and methods). *chato* mutant embryos arrested by E9.0 and remained unturned, with a short anterior-posterior body axis and an open gut tube (Fig. 1; see Fig. S1A,B in the supplementary material).

Analysis of mesodermal tissues in *chato* embryos showed that defects in axis elongation were accompanied by a failure of cells to properly localize with respect to the midline. Analysis of *Twist1* expression, which marks somites and lateral plate mesoderm (Quertermous et al., 1994), showed that these mesodermal tissues were located further away from the midline of *chato* embryos than in wild-type littermates (Fig. 1A,B). Expression of a *Nodal-lacZ* reporter (Collignon et al., 1996b) also showed that the lateral plate mesoderm in *chato* mutants was shorter and wider than in wild-type embryos (Fig. 1C,D). Somitic mesoderm was specified in all *chato* mutants, but it showed defects in morphogenesis (Fig. 1A,B,E,F). Many *chato* embryos ($n$=61/184) showed condensed somites that were mediolaterally expanded and narrow in the anterior-posterior axis, as shown by expression of *Meox1* (Candia et al., 1992) (Fig. 1E,F and Fig. 3C-E). Mesodermal precursors of the heart, which arise from lateral positions, failed to migrate and fuse at the midline of all *chato* mutants and remained in two separate domains at both sides of the embryo as shown by expression of the heart marker *Nkx2.5* (Fig. 1G,H) (Lints et al., 1993); this cardia bifida phenotype is presumably responsible for the death of the embryos at E9.5-10. Altogether, these mesodermal defects are similar to those seen in zebrafish embryos in which convergent extension is disrupted (Matsui et al., 2005), but are different than those of mouse non-canonical Wnt pathway mutants.

### Morphogenetic defects in the *chato* neural plate and notochord

Epithelial tissues in *chato* embryos also had morphogenetic defects. The *chato* headfolds failed to fuse to form a neural tube (Fig. 2A-G). In the open neural plate, markers of specific cell-type populations, such as *Krox20* (*Egr2*) (Wilkinson et al., 1989), were expressed in domains that were narrow along the anterior-posterior axis and laterally expanded when compared with wild-type littermates (Fig. 2A,B), a phenotype similar to zebrafish *vangl2* mutants (Jessen et al., 2002). The neural tube also failed to close normally at more-posterior positions of the anterior-posterior axis. In some *chato* mutants, it completely failed to close (55%, Fig. 2E), whereas in

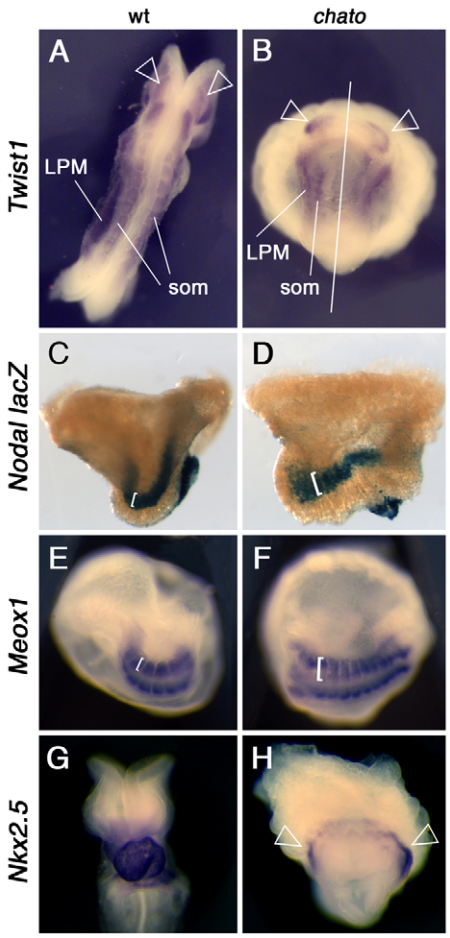


**Fig. 1. Mesoderm defects in *chato* embryos.** Wild-type (wt) (**A**,**C**,**E**,**G**) and *chato* mutant (**B**,**D**,**F**,**H**) mouse embryos were assayed by in situ hybridization with markers expressed in head mesenchyme/lateral plate mesoderm/somitic mesoderm (*Twist1*; A,B, dorsal and ventral views, respectively), somites (*Meox1*; E,F, ventrolateral views) and cardiac mesoderm (*Nkx2.5*; G,H, ventral views). Staining for β-galactosidase activity from a *Nodal-lacZ* reporter labeled lateral plate mesoderm and node of wild-type (C) and *chato* mutant (D) embryos (lateral views). Thirty-three percent of *chato* mutants ($n$=184) had condensed somites that appeared narrow and laterally extended (F). In 52% of *chato* embryos ($n$=184), somites were not clearly discernible morphologically, but somite markers *Twist1* and *Meox1* marked some imperfectly shaped somites. Only 15% of *chato* mutants showed normal somites. Arrowheads in A,B point to head mesenchyme. Brackets in C,D highlight the different width of the lateral plate mesoderm in wild-type and *chato* mutant embryos. Brackets in E,F highlight the different width of the somites. Arrowheads in H mark the cardiac mesoderm in *chato* mutants. LPM, lateral plate mesoderm; som, somites.

others it remained open only at some locations (45%, Fig. 2D), as visualized by expression of the pan-neural marker *Sox2* (Collignon et al., 1996a). Failure to close the neural tube is a characteristic phenotype of zebrafish and *Xenopus* convergent extension conditions (Darken et al., 2002; Goto and Keller, 2002; Wallingford and Harland, 2002), as well as of mouse mutants in components of non-canonical Wnt signaling (*Lp*; Fig. 2H) (reviewed by Copp et al., 2003).

The basis of the defects in neural tube closure appeared, however, to be different between *chato* embryos and non-canonical Wnt pathway mutants. It is believed that the underlying cause of neurulation defects in *Lp* embryos is the abnormally wide floor plate, which might impair the formation of the medial hinge point and the apposition of the neural folds (Greene et al., 1998). The floor plate ventral hinge was morphologically normal in *chato* mutants (Fig. 2F,G). In addition, other markers of territories along the dorsal-ventral neural axis, including *Shh* (Echelard et al., 1993), *Foxa2* (Ruiz i Altaba et al., 1993) and *Olig2* (Zhou et al., 2001), were expressed in regions comparable to those of wild-type littermates (not shown).

*chato* embryos also showed other phenotypic differences from non-canonical Wnt signaling mutants. The notochord, a mesendoderm-derived tissue, is wider in fish, frog and mouse embryos in which the activity of this pathway is disrupted (Goto and Keller, 2002; Greene et al., 1998; Hammerschmidt et al., 1996). Analysis of brachyury (*T*) expression (Wilkinson et al., 1990) in whole-mount *chato* embryos at E8.5 revealed that the notochord was disrupted and was wider than in wild-type littermates in some regions, but narrower or absent in other positions (Fig. 2I,J). In transverse sections, analysis of *T* expression indicated that the characteristic notochord rod present in wild-type embryos at these stages had not been formed in *chato* mutants and, instead, the notochord was still part of the mesendoderm layer (Fig. 2F,G). Therefore, although the notochord irregularities of *chato* mutants indicate defects in the reorganization of this tissue, these defects are different than those of non-canonical Wnt signaling mutants (Fig. 2H).

## *chato* does not genetically interact with non-canonical Wnt signaling mutants

To assess whether *chato* affected the activity of the non-canonical Wnt pathway, we tested for genetic interactions between *chato* and *Lp*. Mouse mutant embryos that lack Lp (Vangl2) display some of the hallmarks of convergent extension mutants, including a wider notochord and failure to close the neural tube (Greene et al., 1998; Murdoch et al., 2001a). *Lp* mutants show strong genetic interactions with other mutations that affect non-canonical Wnt signaling. For example, embryos that are doubly heterozygous for *Lp* and scribbled [*Scrib*; also known as circletail (*Crc*)] (*Lp*/+; *Crc*/+) (Murdoch et al., 2001b) or for *Lp* and *Ptk7* (*Lp*/+; *Ptk7*/+) (Lu et al., 2004), as well as $Lp^{+/-}$; $Dvl1^{+/-}$; $Dvl2^{-/-}$ embryos (Wang, J. et al., 2006), all show the same neural tube closure defects seen in *Lp* homozygous embryos. By contrast, we found that $Lp^{+/-}$; $chato^{+/-}$ double heterozygous animals were viable and fertile and had the curled tail typical of *Lp* heterozygotes (see Fig. S2 in the supplementary material). We also mated double heterozygous carriers to obtain more-severe mutant combinations and evaluated their phenotypes in mesoderm, neural tube and notochord. We did not observe any modification of the *Lp* mutant phenotype in embryos lacking one copy of *chato* ($Lp^{-/-}$; $chato^{+/-}$). Similarly, the *chato* mutant phenotype did not change in the absence of one copy of *Lp* ($Lp^{+/-}$; $chato^{-/-}$). *Lp-chato* double mutant embryos ($Lp^{-/-}$; $chato^{-/-}$) showed characteristics of both *chato* and *Lp* mutants, including elongated somites and an open neural tube (see Fig. S2 in the supplementary material). The lack of genetic interaction between the two mutants does not support a role of *chato* in non-canonical Wnt signaling.

To further test whether *chato* interferes with non-canonical Wnt signaling, we assayed expression of components of this pathway in *chato* mutants. We found that *Vangl1*, *Vangl2*, *Celsr1*, frizzled 3 (*Fzd3*), *Dvl1*, *Dvl2* and *Prickle1* were all expressed in *chato* mutants

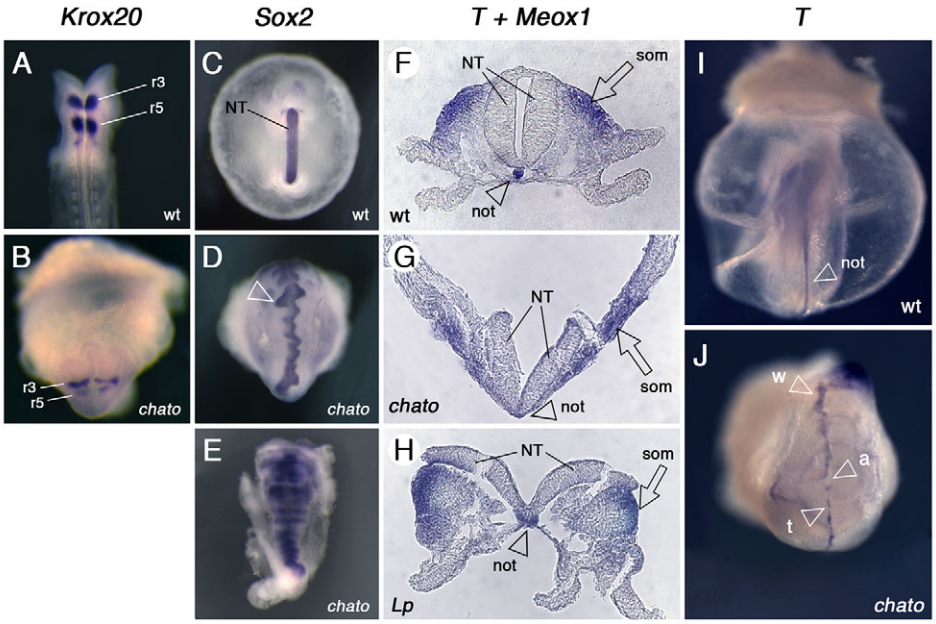


**Fig. 2. Defects in the neural epithelium and notochord of *chato* embryos.** Wild-type (**A**,**C**,**F**,**I**), *chato* (**B**,**D**,**E**,**G**,**J**) and *Lp* mutant (**H**) mouse embryos at E8.5 were assayed by in situ hybridization with markers expressed at rhombomeres 3 and 5 (*Krox20*; A,B, dorsal and ventral views, respectively), neuroepithelia (*Sox2*; C-E, ventral views), somites (*Meox1*; F-H, transverse sections) and notochord (*T*; F-H, transverse sections; I,J, posterior and ventral views, respectively). In some *chato* mutants, parts of the neuroepithelium remained open (arrowhead in D), giving the neural tube a wavy appearance. Transverse sections in F-H were hybridized with probes for both *T* (arrowheads) and the somitic marker *Meox1* (arrows). In *chato* mutants, the notochord was embedded in the mesendoderm layer (arrowhead in G) and never formed an individualized rod (arrowhead in F). The notochord of *Lp* mutants is wider than that of wild-type embryos (F-H, arrowheads) (Greene et al., 1998). Expression of *T* in *chato* mutants (J) shows areas where the notochord was wider (w), thinner (t) or absent (a) as compared with wild-type embryos (I, arrowhead). NT, neural tube; not, notochord; r3, rhombomere 3; r5, rhombomere 5; som, somitic mesoderm.

(see Fig. S3A-H in the supplementary material; data not shown) in the same tissues as in wild-type control embryos (see Fig. S3A-H in the supplementary material) (Crompton et al., 2007; Torban et al., 2006). Reciprocally, *chato* expression was unaltered in *Lp* mutants (see Fig. S3I,J in the supplementary material). Since none of our experiments supports an interaction between *chato* and non-canonical Wnt signaling, we speculate that the morphogenetic defects of *chato* and *Lp* mutants might arise through different molecular mechanisms.

## The *chato* mutation disrupts Zfp568, a novel KRAB zinc-finger protein

Meiotic recombination mapping localized the *chato* mutation to an interval of 209 kb on the proximal region of chromosome 7 (Materials and methods). Sequence analysis of all six genes in this interval revealed a single change: a missense mutation in *Zfp568*, which encodes a member of the Krüppel-associated box (KRAB) domain zinc-finger protein family. KRAB zinc-finger proteins represent one of the largest families of transcriptional regulators in mammals, including ~290 genes (Urrutia, 2003). Members of this family contain a variable number of zinc-finger domains, which are believed to provide DNA-binding specificity to different targets (Gebelein and Urrutia, 2001), and one or several KRAB domains, which have strong transcriptional repressor activity (Margolin et al., 1994).

The missense mutation in the *chato* allele causes a Leu to Pro change in the first of the two KRAB domains of Zfp568 (Fig. 3A,B). This change maps to a highly conserved position within the KRAB domain required for transcriptional repression in COS-1 cells (Margolin et al., 1994). To confirm that mutation of *Zfp568* is responsible of the *chato* mutant phenotype and to test whether the missense mutation disrupted activity of Zfp568 completely, we generated mutant mice from the BayGenomics gene-trap clone RRU161. This gene-trap insertion generates a truncated Zfp568 protein of 11 amino acids that lacks all functional domains, and should represent a null allele of *Zfp568* (Fig. 3A). Both $Zfp568^{chato}/Zfp568^{RRU161}$ and $Zfp568^{RRU161}$ homozygous embryos recapitulated the *chato* phenotype (Fig. 3C-F). Thus, the complementation test indicated that the ENU-induced *chato* mutation is a null allele of *Zfp568*.

*Zfp568* (*chato*) showed a broad expression pattern during embryogenesis (Fig. 3G-L). At E7.5, *chato* was expressed in all cell types as assessed by in situ hybridization in whole-mount embryos and in sections (Fig. 3G,H). At later stages, expression was also ubiquitous in extraembryonic and embryonic tissues (Fig. 3J,L). Expression was highest in the extraembryonic ectoderm (Fig. 3G,J, arrowheads).

## *chato* mutants fail to undergo convergent extension of definitive endoderm

Characterization of the cellular basis of the *chato* axis elongation defects was complicated by the architecture of the E8.5 mouse embryo, which consists of several cellular layers, some of which (e.g. the neuroepithelium) are folded. Compared with other germ layers, we found that the simple epithelial structure of the definitive endoderm made it amenable to straightforward and reliable analysis during the stages of axis elongation. Definitive endoderm cells arise from the primitive streak during gastrulation and form an epithelial

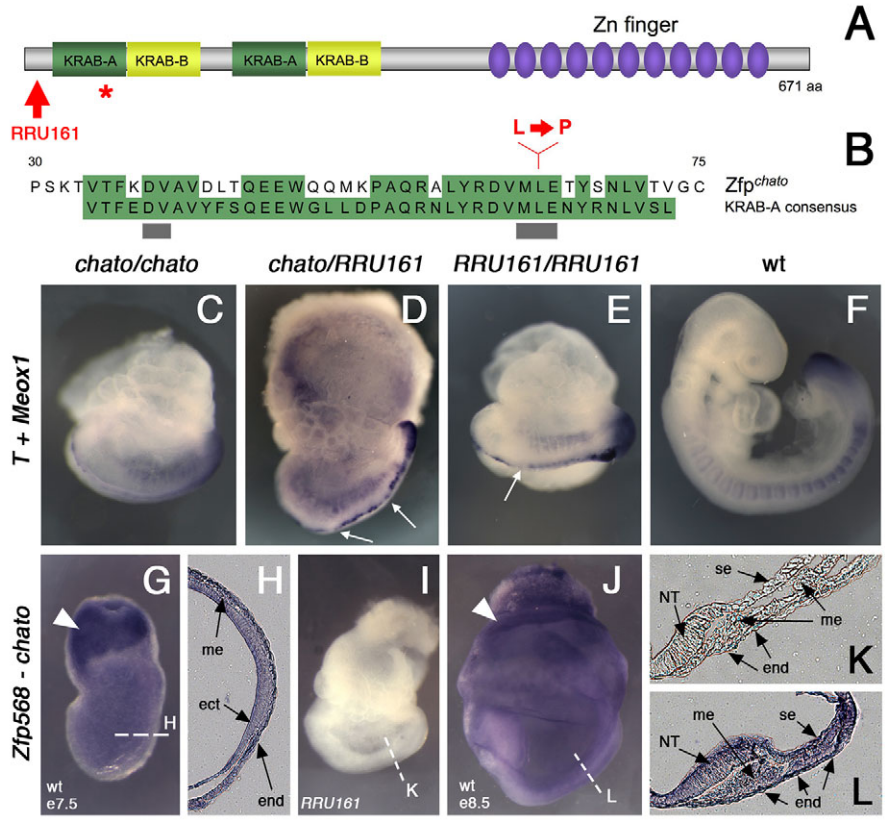


**Fig. 3. The *chato* mutation disrupts *Zfp568*.** (**A**) Domain structure of mouse Zfp568, containing two KRAB-A (green)/KRAB-B (yellow) domains and eleven zinc fingers (purple). The red asterisk marks the position of the *chato* point mutation. The red arrow points to the truncation caused by the *RRU161* gene-trap. (**B**) Sequence comparison of the first KRAB-A domain of Zfp568/Chato with the KRAB-A consensus. Conserved residues are highlighted in green. Gray bars underline residues required for transcriptional repression (Margolin et al., 1994). Red letters indicate the Leu to Pro change caused by the *chato* point mutation. (**C-F**) Complementation test between *chato* and *RRU161* gene-trap alleles. Wild-type (F) and mutant embryos of the allele combinations indicated (C-E) were assayed by in situ hybridization with *T* and *Meox1* probes. The overall embryonic morphology, as well as defects in somites and midline, are indistinguishable between the different *Zfp568* allele combinations. Notochord expression of *T* was irregular, showing a variable width and interruptions (arrows in D,E). (**G-L**) In situ hybridization with a *Zfp568* probe on wild-type embryos at E7.5 (G,H) and E8.5 (J,L). *RRU161* mutant embryos, which generate truncated *Zfp568* transcripts, were used as negative controls (I,K). *Zfp568* is expressed in all embryonic and extraembryonic tissues, as confirmed in transverse sections (H,K,L). *Zfp568* was expressed at higher levels in the extraembryonic ectoderm (arrowheads). NT, neural tube; me, mesoderm; ect, ectoderm; end, endoderm; se, surface epithelia.

monolayer that is continuous with the extraembryonic visceral endoderm (VE) on the exterior of the embryo after E8.0 (reviewed by Lewis and Tam, 2006).

We measured the overall dimensions of the definitive endoderm in wild-type and *chato* mutant embryos during the stages of anterior-posterior axis elongation. Definitive endoderm and VE cells can be discriminated using markers expressed exclusively in the VE, such as transthyretin (*Ttr*) (Cereghini et al., 1992). At E7.5, some VE cells were still present in the embryonic region (Fig. 4A,B, arrowhead). After E8.0 (0-somite stage), the definitive (*Ttr*-negative) endoderm covered the entire embryonic region (Fig. 4C-J). Posterior views of wild-type embryos marked with *Ttr* revealed that the definitive endoderm narrowed between E8.0 and E9.5 (Fig. 4). Measurements of definitive endoderm in wild-type embryos showed that the total length of the definitive endoderm increased 50% between 0-somite and 10-somite stage embryos (Fig. 4K, blue columns; Fig. 5H). At the same stages, definitive endoderm width, measured as the lateral distance across the center of the embryo (Fig. 4H, red line), decreased 2.7-fold (Fig. 4K, green columns; Fig. 5H). These measurements demonstrate that elongation of the definitive endoderm of the wild-type mouse embryo is accompanied by narrowing of the tissue, and thus definitive endoderm undergoes convergent extension.

At early E8.5 (2- to 4-somite stage), the length of the *chato* definitive endoderm was not significantly different from that of wild-type littermates ($P$=0.31), but its width was 1.23-fold that of the wild type ($P$=0.019, Fig. 5F,H). At the 5- to 7-somite stage, the definitive endoderm of *chato* mutants was 14% shorter ($P$=0.031) and twice as wide ($P$=0.0002) as that of wild-type embryos of the same stage (Fig. 5E,F,H). The length and width measurements indicated that the *chato* mutant endoderm grew in both dimensions (Fig. 5E-H). However, the length-to-width ratio (LWR) of *chato* embryonic endoderm did not significantly change between the 2- to 4-somite and the 5- to 7-somite stages ($P$=0.23, Fig. 5G, red columns), whereas the wild-type LWR more than doubled ($P$=0.0007, Fig. 5G, gray columns). By the 5- to 7-somite stage, the LWR of wild-type definitive endoderm was 2.6-fold greater than that of *chato* mutants ($P$=0.0022, Fig. 5G). Thus, convergent extension of the mouse definitive endoderm requires the activity of the Chato protein.

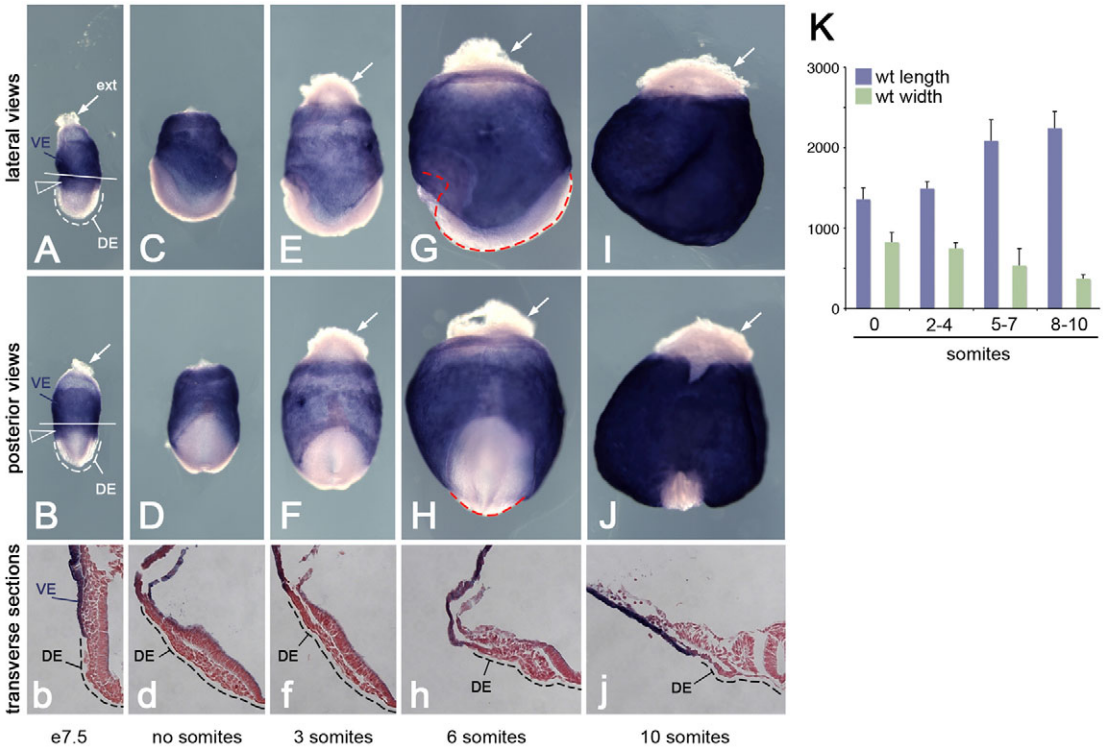


**Fig. 4. Convergent extension in wild-type definitive endoderm.** Whole-mount in situ hybridization with *Ttr* probes of wild-type mouse embryos at E7.5 (**A**,**B**), E8.0 (**C-F**) and E8.5 (**G-J**). Lateral and posterior views illustrate how definitive endoderm (white) grows along the anterior-posterior axis (length) and narrows laterally (width). *Ttr* highlights the extraembryonic visceral endoderm (VE). The white tissue covering the embryonic region corresponds to definitive endoderm (DE). Arrows point to white extraembryonic tissue (ext). All images are at the same magnification. At E7.5, some VE cells (arrowhead in A,B) still overlay the exterior of the embryonic region; the line in A,B delimits embryonic-extraembryonic parts. Gut closure prevented visualization of all the definitive endoderm in I and J. (**b**,**d**,**f**,**h**,**j**) Representative transverse sections of the embryos in the columns above, counterstained with Fast Red. Sections correspond to intermediate levels along the anterior-posterior axis. Only half of each section is shown (midline at the right edge of panel). (**K**) Plot of length (blue) and width (green) definitive endoderm measurements in wild-type embryos of different stages; data in μm. Dimensions of the endoderm were taken as exemplified by dashed lines in G,H. Note that measurements were taken in non-*Ttr*-stained embryos, in which transparency of the tissue allowed for accurate measurements of the whole definitive endoderm. Error bars indicate s.d. See Fig. 5H for primary data.

## Elongation and narrowing of the wild-type definitive endoderm is coupled to cell rearrangements

Convergent extension in zebrafish and *Xenopus* embryos depends on cell rearrangements, including mediolateral cell intercalation and polarized cell migration, which contribute to a decrease in the number of cells across the width of the embryo and to an increase in the number of cells along the anterior-posterior axis (reviewed by Wallingford et al., 2002). We therefore evaluated variations in the number of cells across the width of the mouse definitive endoderm to assess the contribution of cell rearrangements to convergent extension of the mouse endoderm.

We quantified the number of cells across the width of the definitive endoderm at different developmental stages by counting the number of Fast Red-stained nuclei in the outermost layer of transverse sections from E8.0 (0 somites) to E9.0 (10 somites) wild-type embryos (Fig. 4b,d,f,h,j). In headfold stage embryos (E8.0; 0-4 somites), the definitive endoderm layer was 47±6 cells wide at intermediate positions of the anterior-posterior axis (Fig. 6A,B). In 5- to 10-somite embryos, the number of definitive endoderm cells across the width of the embryo decreased to 32±6 cells ($P$<0.0001, Fig. 6A,B). This decrease in cell number correlated with the dramatic narrowing of the definitive endoderm that occurred between these stages (compare Fig. 4D,F,H,J).

A decrease in the number of cells across the width of the definitive endoderm could be the result of mediolateral cell intercalation. However, this number could also be influenced by proliferation, apoptosis and delamination of cells from the primitive streak. To evaluate the contribution of cell proliferation, we assayed the frequency of mitotic cells in transverse sections of the definitive endoderm using phospho-histone H3 antibodies (Fig. 7A,C, green signal). Between E8.0 (0 somites) and E9.0 (10 somites), the definitive endoderm contained 0-3 proliferating cells per section at all levels along the anterior-posterior axis where the gut remained open ($n$=21 embryos/380 sections, Fig. 7A,C and data not shown). By contrast, other embryonic tissues, such as the mesoderm or neuroepithelia, showed a higher mitotic index (Fig. 7A,C). Our results confirm previous reports indicating that the definitive endoderm is a relatively quiescent tissue during early developmental stages (Tremblay and Zaret, 2005) and indicate that the rate of proliferation in the endoderm plays a minor role in the growth of the definitive endoderm during these stages. We did not observe any apoptotic cells in the definitive endoderm at any of the stages analyzed (data not shown). Delamination of cells from the primitive streak plays important roles in the growth of the definitive endoderm at gastrulation stages (Lewis and Tam, 2006). Therefore, during the stages of anterior-posterior axis elongation, the number of cells in the endoderm might increase owing to the continued delamination

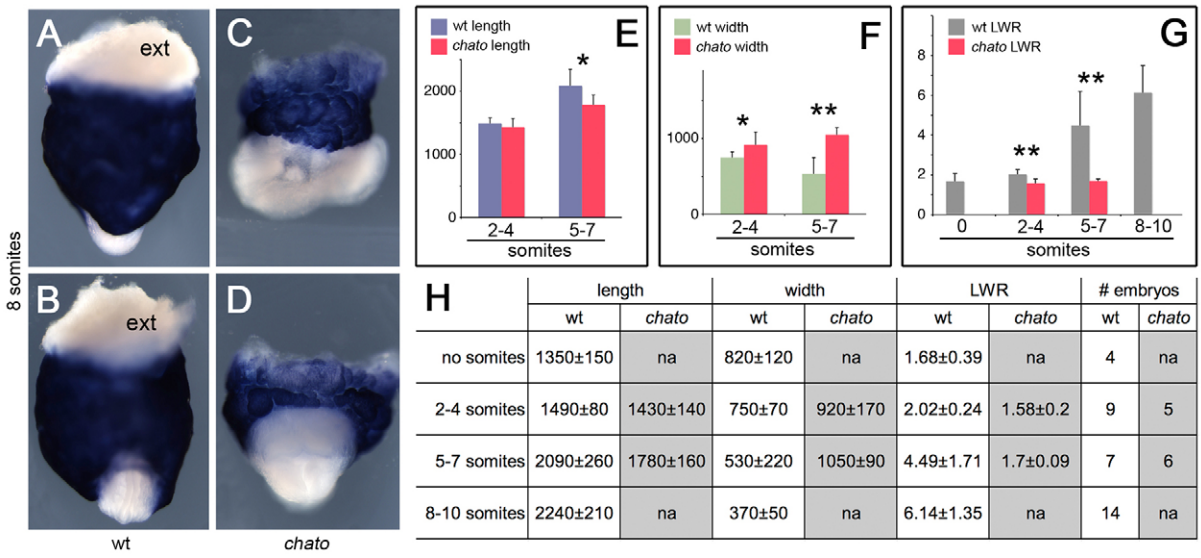


H

| | length | | width | | LWR | | # embryos | |
|---|---|---|---|---|---|---|---|---|
| | wt | *chato* | wt | *chato* | wt | *chato* | wt | *chato* |
| no somites | 1350±150 | na | 820±120 | na | 1.68±0.39 | na | 4 | na |
| 2-4 somites | 1490±80 | 1430±140 | 750±70 | 920±170 | 2.02±0.24 | 1.58±0.2 | 9 | 5 |
| 5-7 somites | 2090±260 | 1780±160 | 530±220 | 1050±90 | 4.49±1.71 | 1.7±0.09 | 7 | 6 |
| 8-10 somites | 2240±210 | na | 370±50 | na | 6.14±1.35 | na | 14 | na |

**Fig. 5. Failure of convergent extension in the definitive endoderm of *chato* mutants.** (**A-D**) Wild-type (A,B) and *chato* mutant (C,D) 8-somite stage mouse embryos hybridized with *Ttr* probes to highlight extraembryonic visceral endoderm (blue) and definitive endoderm (exterior layer of embryonic tissues in white). ext, white extraembryonic tissue. (A,C) Lateral views; (B,D) anterior views. (**E-G**) Plots of (E) wild-type (blue) and *chato* (red) definitive endoderm length (μm), (F) wild-type (green) and *chato* (red) definitive endoderm width (μm), and (G) definitive endoderm length-to-width ratio (LWR) in wild-type (gray) and *chato* mutant (red) embryos. Error bars indicate s.d. **P*<0.05, ***P*<0.01. (**H**) Length and width average measurements ±s.d. in μm. The number of embryos analyzed for each stage is indicated (# embryos); na, not assayed.

of cells from the primitive streak, with a minor contribution from cell proliferation. Because we did not observe apoptosis in the endoderm, we conclude that cellular rearrangements (mediolateral cell intercalation or polarized cell migration) must be responsible for the observed decrease in the number of cells across the width of the definitive endoderm and for the decrease in the width of the tissue.

### *chato* mutants fail to undergo the cell rearrangements required for definitive endoderm convergent extension

We also analyzed rearrangements of cells in the definitive endoderm of *chato* mutants using the approaches described above. Headfold stage (0-4 somites) *chato* mutants had approximately the same cell number across the width of the definitive endoderm as wild-type littermates (Fig. 6A,B). At the 5- to 7-somite and 8- to 10-somite stages, *chato* embryos contained on average ~70% more cells across the width of the definitive endoderm than wild-type embryos (*P*<0.0001, Fig. 6A,B), paralleling the increased width of the definitive endoderm in *chato* mutants (Fig. 5B,D). The rate of cell proliferation (*n*=3 embryos/56 sections) in the definitive endoderm of *chato* mutants was similar to that of the wild type (Fig. 7B-D). Also, no apoptosis was observed in the *chato* mutant endoderm and we did not detect any abnormality in the delamination of definitive endoderm from the primitive streak or in the migration of definitive endoderm cells at gastrulation (see Fig. S1C-F in the supplementary material). Therefore, we conclude that the definitive endoderm is wide in *chato* mutants because normal function of the *chato* gene is required for the cells to rearrange into a longer, narrower structure.

## DISCUSSION

### Convergent extension in the definitive endoderm of the mouse embryo depends on Chato

Although the contribution of convergent extension mechanisms to the elongation of zebrafish and *Xenopus* embryos has been well studied, evidence for a role for convergent extension in mammalian embryogenesis has been limited to the notochord and neural tube (Wang, J. et al., 2006; Yamanaka et al., 2007; Ybot-Gonzalez et al., 2007). Based on embryo morphology and the pattern of expression of

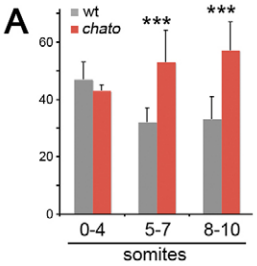


B

| | Cell number | | # embryos | | # sections | |
|---|---|---|---|---|---|---|
| | wt | *chato* | wt | *chato* | wt | *chato* |
| 0-4 somites | 47 ±6 | 43 ±2 | 8 | 2 | 52 | 15 |
| 5-7 somites | 32 ±5 | 53 ±11 | 5 | 6 | 58 | 59 |
| 8-10 somites | 33 ±8 | 57 ±10 | 2 | 4 | 22 | 43 |

**Fig. 6. Cell number changes across the width of the definitive endoderm.** (**A**) Plot of the average definitive endoderm cell number in wild-type (gray) and *chato* mutant (red) mice. Cells were counted in sections of the definitive endoderm stained with Fast Red at medial levels along the anterior-posterior axis (see Fig. 4). Error bars indicate s.d. (**B**) Average number of cells ±s.d. The total number of sections counted for each condition is indicated (# sections); na, not assayed. ****P*<0.0001.

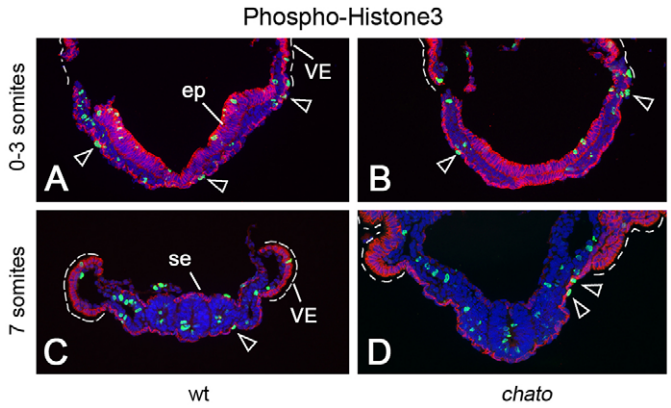


**Fig. 7. Proliferation in definitive endoderm.** Cryosections of wild-type (**A**,**C**) and *chato* mutant (**B**,**D**) mouse embryos at different embryonic stages were labeled with anti-E-cadherin (red) and phospho-histone H3 (green) antibodies. Mitotic cells (green) in the definitive endoderm (highlighted in red by localization of E-cadherin) are indicated by arrowheads. E-cadherin is also present in E7.5 epithelia (ep), embryonic surface ectoderm (se) and extraembryonic visceral endoderm (VE, dashed line). Proliferation of mesoderm and epithelial tissues was not significantly different between wild-type ($n$=21 embryos/380 sections) and *chato* mutant ($n$=3 embryos/56 sections) embryos at these stages.

molecular markers, *chato* mutants appear to have global defects in elongation of the body axis, with abnormalities in the neural plate, paraxial mesoderm, lateral plate mesoderm and definitive endoderm.

To test definitively whether *chato* affects convergent extension, we examined the morphogenesis of the definitive endoderm, a single-layered cell sheet that can be analyzed reliably. Our morphometric analysis provides evidence that the wild-type mouse definitive endoderm undergoes convergent extension. The definitive endoderm begins to narrow and elongate in headfold stage embryos and continues to do so until ~14-somite stage embryos, when definitive endoderm closes to form the gut tube. From the 0- to 10-somite stages, the width of the wild-type definitive endoderm narrows 2.6-fold (from 820 to 310 mm); at the same time it elongates 2-fold. Although delamination of cells from the primitive streak probably contributes to the elongation of the definitive endoderm, the cell rearrangements that we observed are likely to account for the narrowing of the definitive endoderm and to contribute to the anterior-posterior elongation of this tissue. By contrast, the definitive endoderm does not narrow in *chato* embryos. The most dramatic change in dimensions of the definitive endoderm of wild-type embryos occurs between the 2- to 4-somite and 5- to 7-somite stages, when the length-to-width ratio more than doubles; at the same stages, the length-to-width ratio of the *chato* definitive endoderm does not change significantly. In parallel with the abnormal dimensions of the tissue, the *chato* mutation disrupts cell rearrangements in the definitive endoderm. We therefore conclude that the cell rearrangements that depend on Chato are responsible for convergent extension of the definitive endoderm.

The mechanisms underlying the cell rearrangements of convergent extension have been studied in vertebrate and invertebrate embryos. Mediolateral cell intercalation mediates the elongation of *Xenopus* embryos and animal cap explants (Elul et al., 1997; Keller and Tibbetts, 1989; Wilson and Keller, 1991), polarized cell migration is also important for zebrafish convergent extension (Concha and Adams, 1998; Jessen et al., 2002; Warga and Kimmel, 1990), and germ band elongation of *Drosophila* embryos is propelled by the directional generation and resolution of multicellular rosettes (Bertet et al., 2004; Blankenship et al., 2006). One or more of these mechanisms may mediate convergent extension of the mouse definitive endoderm. Because mouse definitive endoderm has an epithelial organization, where cells are held together by adherent apical complexes (Fig. 7, E-cadherin in red), we favor the hypothesis that mediolateral cell intercalation and/or multicellular rosettes, rather than cell migration, mediate definitive endoderm convergent extension. The development of new methods that enable observation of live mouse embryos at cellular resolution will be required to elucidate the precise mechanisms involved.

## Chato is likely to act in convergent extension of all germ layers

Although our studies of convergent extension in *chato* focused on the definitive endoderm, the *chato* phenotype suggests that it also acts in other tissues to regulate convergent extension. Both *chato* lateral plate and somitic mesoderm are shorter in the anterior-posterior axis and wider in the mediolateral dimension than in wild-type embryos, similar to zebrafish convergent extension mutants (Hammerschmidt et al., 1996; Jessen et al., 2002). The neural plate in *chato* fails to close, which could be due to defects in cell rearrangement in this tissue layer. Because *chato* is broadly expressed, it seems likely that it acts autonomously in these tissues to control cell rearrangements. It is, however, possible that convergent extension of the definitive endoderm is required for the migration and/or reorganization of epithelial and mesenchymal tissues.

Most *chato* mutants ($n$=156/184) also show extraembryonic defects, including a ruffled VE (see Fig. S1A,B in the supplementary material). It is therefore possible that these extraembryonic defects could influence the reorganization of definitive endoderm, epithelial and mesenchymal tissues in *chato* mutants. However, the defects in embryonic morphogenesis precede the appearance of extraembryonic phenotypes in *chato* mutants (see Fig. S1C-F in the supplementary material). In addition, 16% of E8.5 *chato* mutants do not show obvious extraembryonic abnormalities but have strong convergent extension phenotypes. Therefore, we favor the hypothesis that the embryonic and extraembryonic defects in *chato* embryos represent distinct, autonomous requirements for *chato*. Further experiments assessing the phenotype of *chato* chimeric embryos or using conditional alleles will define the tissue requirements of this novel KRAB zinc-finger protein.

## The role of the Chato KRAB zinc-finger protein in morphogenesis

The *chato* mutation defines the role of a novel KRAB zinc-finger protein in mammalian convergent extension. Although KRAB domain zinc-finger proteins represent one of the largest gene families in mammals (Urrutia, 2003), only a few mutants have been described. These mutants affect diverse processes, including fertility, pigmentation and embryonic growth (Casademunt et al., 1999; Krebs et al., 2003), but Chato is the first member of this family shown to be required for embryonic morphogenesis. Although the high degree of sequence conservation among members of the family suggests that the genes might be functionally redundant, the severity and specificity of the *chato* phenotype indicates that some KRAB domain proteins have distinct functions.

The KRAB domain seems to be a relatively recent evolutionary feature, as it has only been found in the genomes of tetrapod vertebrates (Urrutia, 2003) (www.ensembl.org). Nevertheless, the C-terminal zinc-finger-containing region of *chato* shows homology to genes found in other animals. The closest homolog of *chato* in

*Drosophila* is *crooked legs* (*crol*), with 39% identity and 53% similarity to the Chato zinc-finger domain. *crol* mutant pupae die with twisted legs that fail to elongate (D'Avino and Thummel, 1998). Although the zebrafish genome does not encode any KRAB domain proteins, morpholinos that disrupt the activity of the zinc-finger gene *bloody fingers* (*blf*) display shortened and widened axial tissue due to defective convergent extension (Sumanas et al., 2005). Blf and Chato share similar zinc-finger domains, but, based on synteny, it is unlikely that Blf is the zebrafish ortholog of Chato. Therefore, it is possible that Chato, Crol and Blf derived from a common ancestral zinc-finger protein that controlled tissue elongation during morphogenesis.

Our results suggest that the Chato KRAB zinc-finger protein acts through a molecular pathway that is independent of non-canonical Wnt signaling. Although mutations in both the mouse *chato* and non-canonical Wnt signaling genes affect convergent extension, their phenotypes are fundamentally different. The defects in axis elongation in the *chato* mesoderm are more profound than those reported in mouse non-canonical Wnt signaling mutants (Figs 1, 2) (Greene et al., 1998; Wang, J. et al., 2006). Most clearly, our analysis shows that *chato* mutants fail to close the gut endoderm and fail to undergo convergent extension in the gut, phenotypes that are not present in *Lp* mutants (data not shown). By contrast, *Lp* mutants have more-dramatic defects in neural tube closure and in convergent extension of the notochord than *chato* mutants (Greene et al., 1998; Wang, J. et al., 2006; Ybot-Gonzalez et al., 2007). A specific role for non-canonical Wnt signaling in morphogenesis of axial tissues is supported by the high level of expression of *Vangl2* and *Vangl1* in the mouse neural tube (Torban et al., 2006; Torban et al., 2008). Altogether, the observations suggest that Chato and non-canonical Wnt signaling act in different tissues and regulate convergent extension through different molecular mechanisms.

Because *chato* mutants are blocked in both definitive endoderm convergent extension and the accompanying cell rearrangements, we conclude that these cell rearrangements drive convergent extension of the mammalian endoderm. KRAB zinc-finger proteins are believed to act as transcriptional repressors (Bellefroid et al., 1991), so Chato might regulate the transcription of genes that regulate specific aspects of cytoskeleton dynamics, components of the extracellular matrix (ECM) or chemotactic clues. Because mutations in mouse genes that have global effects on cytoskeleton organization or the ECM (Garcia-Garcia and Anderson, 2003; George et al., 1993; Rakeman and Anderson, 2006) cause phenotypes dramatically different from those of *chato* mutants, we infer that *chato* controls cellular processes that are specific to convergent extension.

## Chato might act in a common molecular pathway with Hand1 and Yap65

Although the molecular mechanisms that implement Chato function remain to be discovered, additional information might come from the analysis of two other mouse mutants with phenotypes similar to *chato*. Mutants that lack *Hand1*, which encodes a bHLH transcription factor, arrest development at the 9- to 14-somite stage, fail to close the gut endoderm, have a kinked neural plate and show extraembryonic defects similar to those of *chato* embryos (Firulli et al., 1998). Loss of mouse *Yap65* (*Yap1*), which encodes a protein with a proline-rich domain, WW domains, SH3 binding motifs, a coiled-coil and a PDZ binding motif, also causes phenotypes similar to *chato* (Morin-Kensicki et al., 2006). Studies similar to those described here could test whether these mutants have convergent extension defects in epithelia, mesenchyme and endoderm and whether cell rearrangements underlie the *Hand1* and *Yap1* abnormalities. Future experiments will be able to test whether *chato*, *Hand1* and *Yap1* act in a common biochemical process that regulates convergent extension in the mouse.

We thank Andrew Recknagel, Maegan Harden, Nina Lampen and Carole Daugherty for help and technical support; Elizabeth Robertson, Scott Weatherbee, Tristan Rodriguez, Philippe Gros, Andre Goffinet, Tudorita Tumbar and Tony Bretscher for providing mouse strains, reagents and/or use of lab equipment; and Holger Sondermann, Jeffrey Lee and Isabelle Migeotte for helpful discussions and comments on the manuscript. This work was supported by NIH grant HD035455 to K.V.A. and a Basil O'Connor March of Dimes award to M.J.G.G.

**Supplementary material**

Supplementary material for this article is available at
http://dev.biologists.org/cgi/content/full/135/18/3053/DC1

**References**

**Bardet, P. L., Horard, B., Laudet, V. and Vanacker, J. M.** (2005). The ERRalpha orphan nuclear receptor controls morphogenetic movements during zebrafish gastrulation. *Dev. Biol.* **281**, 102-111.

**Bellefroid, E. J., Poncelet, D. A., Lecocq, P. J., Revelant, O. and Martial, J. A.** (1991). The evolutionarily conserved Kruppel-associated box domain defines a subfamily of eukaryotic multifingered proteins. *Proc. Natl. Acad. Sci. USA* **88**, 3608-3612.

**Belo, J. A., Bouwmeester, T., Leyns, L., Kertesz, N., Gallo, M., Follettie, M. and De Robertis, E. M.** (1997). Cerberus-like is a secreted factor with neutralizing activity expressed in the anterior primitive endoderm of the mouse gastrula. *Mech. Dev.* **68**, 45-57.

**Bertet, C., Sulak, L. and Lecuit, T.** (2004). Myosin-dependent junction remodelling controls planar cell intercalation and axis elongation. *Nature* **429**, 667-671.

**Blankenship, J. T., Backovic, S. T., Sanny, J. S., Weitz, O. and Zallen, J. A.** (2006). Multicellular rosette formation links planar cell polarity to tissue morphogenesis. *Dev. Cell* **11**, 459-470.

**Candia, A. F., Hu, J., Crosby, J., Lalley, P. A., Noden, D., Nadeau, J. H. and Wright, C. V.** (1992). Mox-1 and Mox-2 define a novel homeobox gene subfamily and are differentially expressed during early mesodermal patterning in mouse embryos. *Development* **116**, 1123-1136.

**Casademunt, E., Carter, B. D., Benzel, I., Frade, J. M., Dechant, G. and Barde, Y. A.** (1999). The zinc finger protein NRIF interacts with the neurotrophin receptor p75(NTR) and participates in programmed cell death. *EMBO J.* **18**, 6050-6061.

**Cereghini, S., Ott, M. O., Power, S. and Maury, M.** (1992). Expression patterns of vHNF1 and HNF1 homeoproteins in early postimplantation embryos suggest distinct and sequential developmental roles. *Development* **116**, 783-797.

**Collignon, J., Sockanathan, S., Hacker, A., Cohen-Tannoudji, M., Norris, D., Rastan, S., Stevanovic, M., Goodfellow, P. N. and Lovell-Badge, R.** (1996a). A comparison of the properties of Sox-3 with Sry and two related genes, Sox-1 and Sox-2. *Development* **122**, 509-520.

**Collignon, J., Varlet, I. and Robertson, E. J.** (1996b). Relationship between asymmetric nodal expression and the direction of embryonic turning. *Nature* **381**, 155-158.

**Concha, M. L. and Adams, R. J.** (1998). Oriented cell divisions and cellular morphogenesis in the zebrafish gastrula and neurula: a time-lapse analysis. *Development* **125**, 983-994.

**Copp, A. J., Greene, N. D. and Murdoch, J. N.** (2003). The genetic basis of mammalian neurulation. *Nat. Rev. Genet.* **4**, 784-793.

**Crompton, L. A., Du Roure, C. and Rodriguez, T. A.** (2007). Early embryonic expression patterns of the mouse Flamingo and Prickle orthologues. *Dev. Dyn.* **236**, 3137-3143.

**Curtin, J. A., Quint, E., Tsipouri, V., Arkell, R. M., Cattanach, B., Copp, A. J., Henderson, D. J., Spurr, N., Stanier, P., Fisher, E. M. et al.** (2003). Mutation of Celsr1 disrupts planar polarity of inner ear hair cells and causes severe neural tube defects in the mouse. *Curr. Biol.* **13**, 1129-1133.

**D'Avino, P. P. and Thummel, C. S.** (1998). crooked legs encodes a family of zinc finger proteins required for leg morphogenesis and ecdysone-regulated gene expression during Drosophila metamorphosis. *Development* **125**, 1733-1745.

**Darken, R. S., Scola, A. M., Rakeman, A. S., Das, G., Mlodzik, M. and Wilson, P. A.** (2002). The planar polarity gene strabismus regulates convergent extension movements in Xenopus. *EMBO J.* **21**, 976-985.

**Davidson, L. A. and Keller, R. E.** (1999). Neural tube closure in Xenopus laevis involves medial migration, directed protrusive activity, cell intercalation and convergent extension. *Development* **126**, 4547-4556.

**Echelard, Y., Epstein, D. J., St-Jacques, B., Shen, L., Mohler, J., McMahon, J. A. and McMahon, A. P.** (1993). Sonic hedgehog, a member of a family of putative signaling molecules, is implicated in the regulation of CNS polarity. *Cell* **75**, 1417-1430.

**Elul, T. and Keller, R.** (2000). Monopolar protrusive activity: a new morphogenic cell behavior in the neural plate dependent on vertical interactions with the mesoderm in Xenopus. *Dev. Biol.* **224**, 3-19.
**Elul, T., Koehl, M. A. and Keller, R.** (1997). Cellular mechanism underlying neural convergent extension in Xenopus laevis embryos. *Dev. Biol.* **191**, 243-258.
**Firulli, A. B., McFadden, D. G., Lin, Q., Srivastava, D. and Olson, E. N.** (1998). Heart and extra-embryonic mesodermal defects in mouse embryos lacking the bHLH transcription factor Hand1. *Nat. Genet.* **18**, 266-270.
**Garcia-Garcia, M. J. and Anderson, K. V.** (2003). Essential role of glycosaminoglycans in Fgf signaling during mouse gastrulation. *Cell* **114**, 727-737.
**Garcia-Garcia, M. J., Eggenschwiler, J. T., Caspary, T., Alcorn, H. L., Wyler, M. R., Huangfu, D., Rakeman, A. S., Lee, J. D., Feinberg, E. H., Timmer, J. R. et al.** (2005). Analysis of mouse embryonic patterning and morphogenesis by forward genetics. *Proc. Natl. Acad. Sci. USA* **102**, 5913-5919.
**Gebelein, B. and Urrutia, R.** (2001). Sequence-specific transcriptional repression by KS1, a multiple-zinc-finger-Kruppel-associated box protein. *Mol. Cell. Biol.* **21**, 928-939.
**George, E. L., Georges-Labouesse, E. N., Patel-King, R. S., Rayburn, H. and Hynes, R. O.** (1993). Defects in mesoderm, neural tube and vascular development in mouse embryos lacking fibronectin. *Development* **119**, 1079-1091.
**Goto, T. and Keller, R.** (2002). The planar cell polarity gene strabismus regulates convergence and extension and neural fold closure in Xenopus. *Dev. Biol.* **247**, 165-181.
**Greene, N. D., Gerrelli, D., Van Straaten, H. W. and Copp, A. J.** (1998). Abnormalities of floor plate, notochord and somite differentiation in the loop-tail (Lp) mouse: a model of severe neural tube defects. *Mech. Dev.* **73**, 59-72.
**Hammerschmidt, M., Pelegri, F., Mullins, M. C., Kane, D. A., Brand, M., van Eeden, F. J., Furutani-Seiki, M., Granato, M., Haffter, P., Heisenberg, C. P. et al.** (1996). Mutations affecting morphogenesis during gastrulation and tail formation in the zebrafish, Danio rerio. *Development* **123**, 143-151.
**Jessen, J. R., Topczewski, J., Bingham, S., Sepich, D. S., Marlow, F., Chandrasekhar, A. and Solnica-Krezel, L.** (2002). Zebrafish trilobite identifies new roles for Strabismus in gastrulation and neuronal movements. *Nat. Cell Biol.* **4**, 610-615.
**Kasarskis, A., Manova, K. and Anderson, K. V.** (1998). A phenotype-based screen for embryonic lethal mutations in the mouse. *Proc. Natl. Acad. Sci. USA* **95**, 7485-7490.
**Keller, R. and Tibbetts, P.** (1989). Mediolateral cell intercalation in the dorsal, axial mesoderm of Xenopus laevis. *Dev. Biol.* **131**, 539-549.
**Kibar, Z., Vogan, K. J., Groulx, N., Justice, M. J., Underhill, D. A. and Gros, P.** (2001). Ltap, a mammalian homolog of Drosophila Strabismus/Van Gogh, is altered in the mouse neural tube mutant Loop-tail. *Nat. Genet.* **28**, 251-255.
**Kinder, S. J., Tsang, T. E., Quinlan, G. A., Hadjantonakis, A. K., Nagy, A. and Tam, P. P.** (1999). The orderly allocation of mesodermal cells to the extraembryonic structures and the anteroposterior axis during gastrulation of the mouse embryo. *Development* **126**, 4691-4701.
**Krebs, C. J., Larkins, L. K., Price, R., Tullis, K. M., Miller, R. D. and Robins, D. M.** (2003). Regulator of sex-limitation (Rsl) encodes a pair of KRAB zinc-finger genes that control sexually dimorphic liver gene expression. *Genes Dev.* **17**, 2664-2674.
**Lawson, K. A.** (1999). Fate mapping the mouse embryo. *Int. J. Dev. Biol.* **43**, 773-775.
**Lewis, S. L. and Tam, P. P.** (2006). Definitive endoderm of the mouse embryo: formation, cell fates, and morphogenetic function. *Dev. Dyn.* **235**, 2315-2329.
**Lints, T. J., Parsons, L. M., Hartley, L., Lyons, I. and Harvey, R. P.** (1993). Nkx-2.5: a novel murine homeobox gene expressed in early heart progenitor cells and their myogenic descendants. *Development* **119**, 419-431.
**Lu, X., Borchers, A. G., Jolicoeur, C., Rayburn, H., Baker, J. C. and Tessier-Lavigne, M.** (2004). PTK7/CCK-4 is a novel regulator of planar cell polarity in vertebrates. *Nature* **430**, 93-98.
**Margolin, J. F., Friedman, J. R., Meyer, W. K., Vissing, H., Thiesen, H. J. and Rauscher, F. J.** (1994). Kruppel-associated boxes are potent transcriptional repression domains. *Proc. Natl. Acad. Sci. USA* **91**, 4509-4513.
**Matsui, T., Raya, A., Kawakami, Y., Callol-Massot, C., Capdevila, J., Rodriguez-Esteban, C. and Izpisua Belmonte, J. C.** (2005). Noncanonical Wnt signaling regulates midline convergence of organ primordia during zebrafish development. *Genes Dev.* **19**, 164-175.
**Montcouquiol, M., Rachel, R. A., Lanford, P. J., Copeland, N. G., Jenkins, N. A. and Kelley, M. W.** (2003). Identification of Vangl2 and Scrb1 as planar polarity genes in mammals. *Nature* **423**, 173-177.
**Moon, R. T., Campbell, R. M., Christian, J. L., McGrew, L. L., Shih, J. and Fraser, S.** (1993). Xwnt-5A: a maternal Wnt that affects morphogenetic movements after overexpression in embryos of Xenopus laevis. *Development* **119**, 97-111.
**Morin-Kensicki, E. M., Boone, B. N., Howell, M., Stonebraker, J. R., Teed, J., Alb, J. G., Magnuson, T. R., O'Neal, W. and Milgram, S. L.** (2006). Defects in yolk sac vasculogenesis, chorioallantoic fusion, and embryonic axis elongation in mice with targeted disruption of Yap65. *Mol. Cell. Biol.* **26**, 77-87.
**Murdoch, J. N., Doudney, K., Paternotte, C., Copp, A. J. and Stanier, P.** (2001a). Severe neural tube defects in the loop-tail mouse result from mutation of Lpp1, a novel gene involved in floor plate specification. *Hum. Mol. Genet.* **10**, 2593-2601.
**Murdoch, J. N., Rachel, R. A., Shah, S., Beermann, F., Stanier, P., Mason, C. A. and Copp, A. J.** (2001b). Circletail, a new mouse mutant with severe neural tube defects: chromosomal localization and interaction with the loop-tail mutation. *Genomics* **78**, 55-63.
**Nagy, A.** (2003). Manipulating the mouse embryo: a laboratory manual. Cold Spring Harbor, NY: Cold Spring Harbor Laboratory Press.
**Quertermous, E. E., Hidai, H., Blanar, M. A. and Quertermous, T.** (1994). Cloning and characterization of a basic helix-loop-helix protein expressed in early mesoderm and the developing somites. *Proc. Natl. Acad. Sci. USA* **91**, 7066-7070.
**Rakeman, A. S. and Anderson, K. V.** (2006). Axis specification and morphogenesis in the mouse embryo require Nap1, a regulator of WAVE-mediated actin branching. *Development* **133**, 3075-3083.
**Ruiz i Altaba, A., Prezioso, V. R., Darnell, J. E. and Jessell, T. M.** (1993). Sequential expression of HNF-3 beta and HNF-3 alpha by embryonic organizing centers: the dorsal lip/node, notochord and floor plate. *Mech. Dev.* **44**, 91-108.
**Sumanas, S., Zhang, B., Dai, R. and Lin, S.** (2005). 15-zinc finger protein Bloody Fingers is required for zebrafish morphogenetic movements during neurulation. *Dev. Biol.* **283**, 85-96.
**Tada, M. and Smith, J. C.** (2000). Xwnt11 is a target of Xenopus Brachyury: regulation of gastrulation movements via Dishevelled, but not through the canonical Wnt pathway. *Development* **127**, 2227-2238.
**Tada, M., Concha, M. L. and Heisenberg, C. P.** (2002). Non-canonical Wnt signalling and regulation of gastrulation movements. *Semin. Cell Dev. Biol.* **13**, 251-260.
**Tahinci, E. and Symes, K.** (2003). Distinct functions of Rho and Rac are required for convergent extension during Xenopus gastrulation. *Dev. Biol.* **259**, 318-335.
**Torban, E., Wang, H. J., Patenaude, A. M., Riccomagno, M., Daniels, E., Epstein, D. and Gros, P.** (2006). Tissue, cellular and sub-cellular localization of the Vangl2 protein during embryonic development: effect of the Lp mutation. *Gene Expr. Patterns* **7**, 346-354.
**Torban, E., Patenaude, A. M., Leclerc, S., Rakowiecki, S., Gauthier, S., Andelfinger, G., Epstein, D. J. and Gros, P.** (2008). Genetic interaction between members of the Vangl family causes neural tube defects in mice. *Proc. Natl. Acad. Sci. USA* **105**, 3449-3454.
**Tremblay, K. D. and Zaret, K. S.** (2005). Distinct populations of endoderm cells converge to generate the embryonic liver bud and ventral foregut tissues. *Dev. Biol.* **280**, 87-99.
**Urrutia, R.** (2003). KRAB-containing zinc-finger repressor proteins. *Genome Biol.* **4**, 231.
**von der Hardt, S., Bakkers, J., Inbal, A., Carvalho, L., Solnica-Krezel, L., Heisenberg, C. P. and Hammerschmidt, M.** (2007). The Bmp gradient of the zebrafish gastrula guides migrating lateral cells by regulating cell-cell adhesion. *Curr. Biol.* **17**, 475-487.
**Wallingford, J. B. and Harland, R. M.** (2002). Neural tube closure requires Dishevelled-dependent convergent extension of the midline. *Development* **129**, 5815-5825.
**Wallingford, J. B., Rowning, B. A., Vogeli, K. M., Rothbächer, U., Fraser, S. E. and Harland, R. M.** (2000). Dishevelled controls cell polarity during Xenopus gastrulation. *Nature* **405**, 81-85.
**Wallingford, J. B., Fraser, S. E. and Harland, R. M.** (2002). Convergent extension: the molecular control of polarized cell movement during embryonic development. *Dev. Cell* **2**, 695-706.
**Wang, J., Hamblet, N. S., Mark, S., Dickinson, M. E., Brinkman, B. C., Segil, N., Fraser, S. E., Chen, P., Wallingford, J. B. and Wynshaw-Boris, A.** (2006). Dishevelled genes mediate a conserved mammalian PCP pathway to regulate convergent extension during neurulation. *Development* **133**, 1767-1778.
**Wang, Y., Guo, N. and Nathans, J.** (2006). The role of Frizzled3 and Frizzled6 in neural tube closure and in the planar polarity of inner-ear sensory hair cells. *J. Neurosci.* **26**, 2147-2156.
**Warga, R. M. and Kimmel, C. B.** (1990). Cell movements during epiboly and gastrulation in zebrafish. *Development* **108**, 569-580.
**Wilkinson, D. G., Bhatt, S., Chavrier, P., Bravo, R. and Charnay, P.** (1989). Segment-specific expression of a zinc-finger gene in the developing nervous system of the mouse. *Nature* **337**, 461-464.
**Wilkinson, D. G., Bhatt, S. and Herrmann, B. G.** (1990). Expression pattern of the mouse T gene and its role in mesoderm formation. *Nature* **343**, 657-659.
**Wilson, P. and Keller, R.** (1991). Cell rearrangement during gastrulation of Xenopus: direct observation of cultured explants. *Development* **112**, 289-300.
**Yamanaka, Y., Tamplin, O. J., Beckers, A., Gossler, A. and Rossant, J.** (2007). Live imaging and genetic analysis of mouse notochord formation reveals regional morphogenetic mechanisms. *Dev. Cell* **13**, 884-896.
**Ybot-Gonzalez, P., Savery, D., Gerrelli, D., Signore, M., Mitchell, C. E., Faux, C. H., Greene, N. D. and Copp, A. J.** (2007). Convergent extension, planar-cell-polarity signalling and initiation of mouse neural tube closure. *Development* **134**, 789-799.
**Zhou, Q., Choi, G. and Anderson, D. J.** (2001). The bHLH transcription factor Olig2 promotes oligodendrocyte differentiation in collaboration with Nkx2.2. *Neuron* **31**, 791-807.